A 19.1–25.5-GHz Compact Dual-Mode Rotary Traveling-Wave Oscillator With 195.4-dBc/Hz FoM$_T$

Hongkun Li, Yiyang Shu, *Member, IEEE*, Changting Pi, and Xun Luo, *Senior Member, IEEE*

***Abstract*— In this letter, a dual-mode rotary traveling-wave oscillator (RTWO) is proposed to achieve wide operation bandwidth and multiple phases. Two twisted differential transmission lines are coupled together to form the dual-mode traveling-wave resonator. Sixteen pairs of back-to-back inverters and capacitors are connected to the resonators to introduce the multicore multiphase operation. The mode switches are used to control the coupling direction and select the desired mode without degrading the quality factor. Verified in a 40-nm CMOS process, the proposed dual-mode RTWO exhibits a dual-mode frequency range from 19.1 to 25.5 GHz with the core size of 0.08 mm^2. The measured 10-MHz phase noise at 25.30 and 22.12 GHz is −129.6 and −131.5 dBc/Hz, respectively. The best FoM and FoM$_T$ are 186.2 and 195.4 dBc/Hz, respectively.**

***Index Terms*— Dual-mode, mode switching, multiphase, rotary traveling-wave oscillator (RTWO), wideband.**

I. Introduction

RECENTLY, with the pursuit of high speed and multistandard wireless communication such as 5G communication, the design of local oscillator (LO) is facing the challenges of low phase noise, wide tuning range (TR), and low power consumption [1]–[10]. Meanwhile, multiple phases and small area are also desired to support multiphase wireless operation and minimize the cost [11], [12]. Conventional *LC* oscillators (LCOs) generate multiphase signal by coupling multiple oscillators together in sacrifice of more chip area [13]–[19]. It is not easy for coupled LCOs to generate more than four phases. Compared with conventional coupled LCOs, rotary traveling-wave oscillator (RTWO) has the advantage of generating multiple phases in limited area [20]–[25]. However, the reported RTWOs lack effective wideband tuning method and are less attractive to multistandard wireless communication systems.

In this letter, a dual-mode coupled RTWO is proposed and verified in a 40-nm CMOS technology to obtain wide frequency range and multiple phases within a small chip size.

Manuscript received 30 March 2022; revised 30 May 2022; accepted 11 June 2022. Date of publication 23 June 2022; date of current version 8 November 2022. This work was supported in part by the National Key Research and Development Program of China under Grant 2021YFE0205600, in part by the National Natural Science Foundation of China under Grant 62161160310, and in part by the Key Basic Research Project of Shenzhen under Grant JCYJ20210324120004013. *(Corresponding author: Yiyang Shu.)*

The authors are with the Center for Advanced Semiconductor and Integrated Micro-System, University of Electronic Science and Technology of China (UESTC), Chengdu 611731, China (e-mail: yiyang.shu@outlook.com).

Color versions of one or more figures in this letter are available at https://doi.org/10.1109/LMWC.2022.3183446.

Digital Object Identifier 10.1109/LMWC.2022.3183446

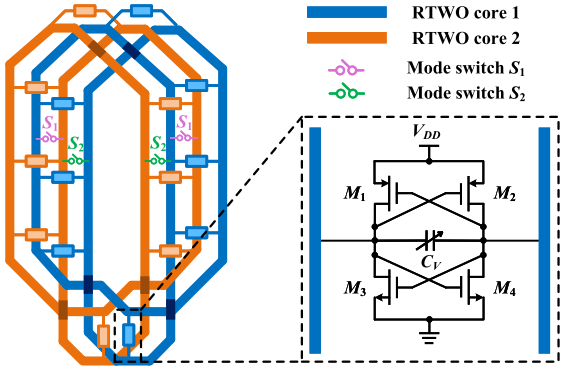

Fig. 1. Configuration of the proposed dual-mode RTWO.

Coupling is formed by nesting two RTWO cores together, and thus additional area can be avoided. The operation bandwidth is extended by dual-mode switching without degrading the quality factor. Meanwhile, the proposed oscillator can achieve high stability in each mode by selecting proper size of mode switches. The measured results exhibit a continuous dual-mode frequency range from 19.1 to 25.5 GHz. Competitive FoM$_T$ of 195.4 dBc/Hz and FoM$_A$ of 197.2 dBc/Hz are obtained.

II. Design of the Dual-Mode RTWO

A single-core RTWO is divided into N segments to support N differential phases [25]. The oscillation frequency is determined by the following equation:

$$f_0 = \frac{1}{2Nl_{\text{seg}}\sqrt{L_0\left(C_0 + \frac{C_V + C_{\text{par}}}{l_{\text{seg}}}\right)}} \tag{1}$$

where l_{seg} represents the length of each segment, L_0 and C_0 are the series inductance and shunt capacitance of transmission line per unit length, respectively, C_V is the tuning capacitance, and C_{par} is the parasitic capacitance of inverter. As implied from (1), the tuning capacitance plays a limited role in the whole capacitance, resulting in a narrow operating bandwidth for conventional RTWO.

To achieve a wide frequency range, Fig. 1 depicts the configuration of the proposed dual-mode RTWO. This structure consists of two mutually nested and coupled RTWO cores. Each RTWO core includes a mobius-ring differential transmission line and eight pairs of back-to-back inverters with tuning capacitors. The mode switches S_1 and S_2 placed between the RTWO cores determine the two modes, respectively.

Fig. 2 shows an unfolded simplified model of the proposed dual-mode RTWO. The voltage wave direction, voltage phase,

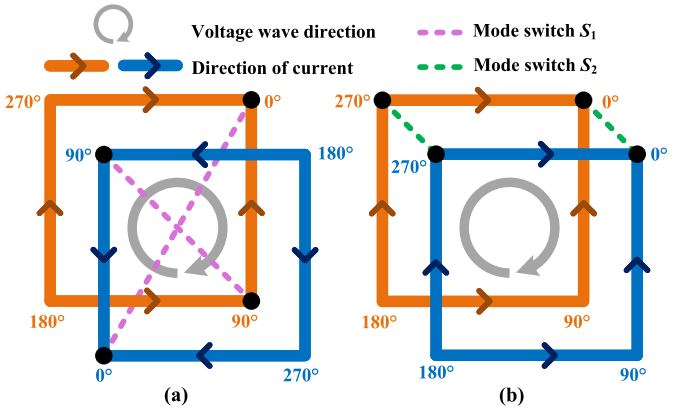

Fig. 2. Simplified operation states of (a) mode-1 and (b) mode-2.

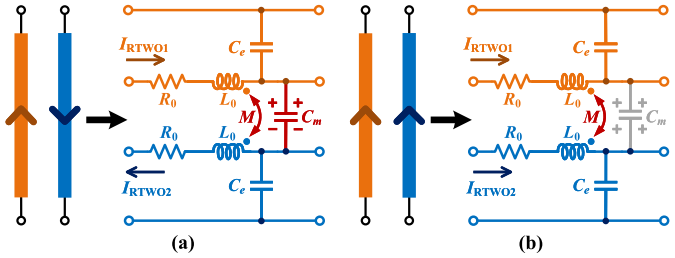

Fig. 3. Transmission line models with coupling in two modes. (a) Mode-1. (b) Mode-2.

and current direction in the different modes are shown to exhibit the operation states of the two modes. The dotted lines present the turned-on switches. S_1 determines mode-1, while S_2 excites mode-2, as shown in Fig. 2(a) and (b), respectively. In each mode, the turned-on mode switches are placed in two positions with a 90° phase difference. It is notable that the symmetry of the structure makes it difficult to predict the startup state of the RTWO. Once the two switches in each mode are connected in differential places, the direction of voltage waves in the two cores cannot be determined [24]. Therefore, the two non-differential switches are necessary in this design. The turned-on switches can synchronize the phases of the connected points, and thus controlling the current distribution on the oscillators, as shown in Fig. 2. In mode-1, the voltage and current waves in the two RTWO cores are in opposite directions. In mode-2, the waves are in-phase. The different wave directions make the equivalent coupling different in each mode, leading to two frequency bands. It is worth mentioning that in each mode, there is no current flowing in the path where the switches locate. Then, the energy loss on the ON-resistance (R_{ON}) is negligible. As a result, the dual-mode operation can effectively avoid the deterioration of the quality factor caused by R_{ON}.

When the waves are activated around the two RTWO rings, there are electric coupling and magnetic coupling between adjacent transmission lines. The transmission line with coupling is modeled in Fig. 3. C_e is the equivalent capacitance per unit length considering the shunt capacitance of transmission line, parasitic capacitance of inverters, and tuning capacitance. C_m represents the electric coupling between transmission lines, while mutual inductance M represents magnetic coupling. As shown in Fig. 3(a), when the proposed dual-mode RTWO operates in mode-1, the currents on coupled transmission lines

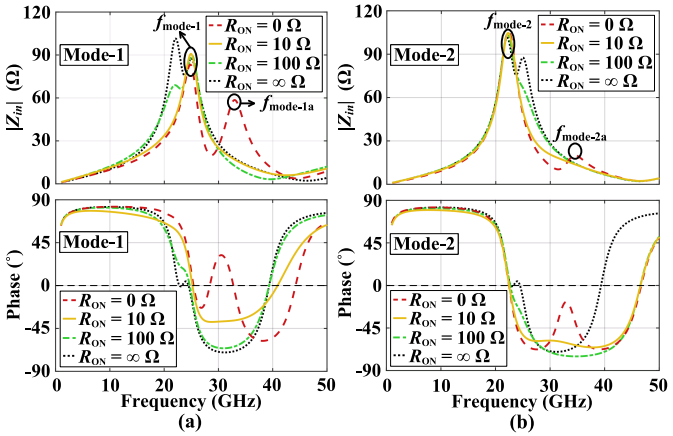

Fig. 4. Simulated input impedance and phase response in (a) mode-1 and (b) mode-2.

are in opposite directions. The magnetic flux generated by each transmission line adds destructively, leading to equivalent inductance per unit length $L_{\text{mode-1}} = L_0 - M$; C_m is excited by the odd-mode voltage at both the ends, so the equivalent shunt capacitance $C_{\text{mode-1}} = C_e + 2C_m$. As shown in Fig. 3(b), once the dual-mode RTWO operates in mode-2, the electric coupling and magnetic coupling are excited in even mode, so $L_{\text{mode-2}} = L_0 + M$, $C_{\text{mode-2}} = C_e$. According to (1), the oscillation frequency of the proposed RTWO in mode-1 and mode-2 can be derived as

$$f_{\text{mode-1}} = \frac{1}{2Nl_{\text{seg}}\sqrt{(L_0 - M)(C_e + 2C_m)}} \tag{2}$$

$$f_{\text{mode-2}} = \frac{1}{2Nl_{\text{seg}}\sqrt{(L_0 + M)C_e}}. \tag{3}$$

Considering that magnetic coupling M is stronger than electric coupling C_m, $f_{\text{mode-1}}$ and $f_{\text{mode-2}}$ correspond to a higher and lower frequencies, respectively. Fig. 4 displays the simulated input impedance and phase response seen from differential ports. There are two peaks located at $f_{\text{mode-1}}$ and $f_{\text{mode-2}}$ which contain no mode switches (i.e., $R_{ON} = \infty\ \Omega$). Bimodal oscillation may occur if the negative resistance provided by the inverters is large enough. As shown in Fig. 4(a) and (b), a small R_{ON} can damp input impedance and avoid phase response crossing zero at undesired resonant frequencies [7]. The simulated results show that bimodal oscillation can be avoided when R_{ON} is smaller than 100 Ω.

It is notable that R_{ON} is not always as small as possible. Fig. 4 also shows that the proposed dual-mode RTWO produces an additional peak of input impedance at $f_{\text{mode-1a}}$ and $f_{\text{mode-2a}}$ when ideal switches (i.e., $R_{ON} = 0\ \Omega$) are used. Unlike LC-type mode-switching oscillator, the proposed dual-mode RTWO has additional resonant paths through switches at such additional frequencies, as shown in Fig. 5. The additional paths can create new stability problems and deteriorate the performance of oscillating ring. Thus, this phenomenon defines the lower bound for R_{ON}. According to simulation, the additional peaks in both modes can be suppressed when R_{ON} is larger than 10 Ω. Once R_{ON} is set from 10 to 100 Ω, it hardly changes the phase noise of the oscillator.

III. Circuit Implementation

The proposed dual-mode RTWO has been implemented in a 40-nm CMOS technology. The coupled transmission lines

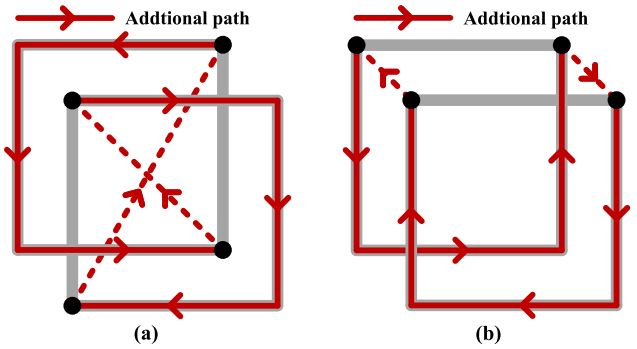

Fig. 5. Additional oscillation path when using ideal switches in (a) mode-1 and (b) mode-2.

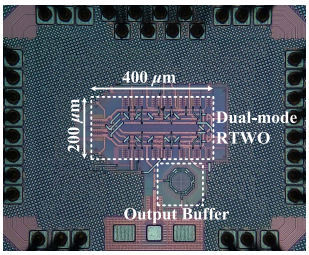

Fig. 6. Die micrograph of the proposed dual-mode RTWO.

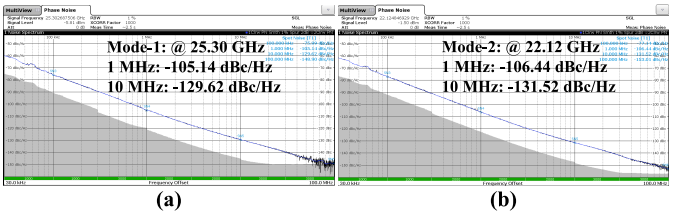

Fig. 7. Measured phase noise in (a) mode-1 and (b) mode-2.

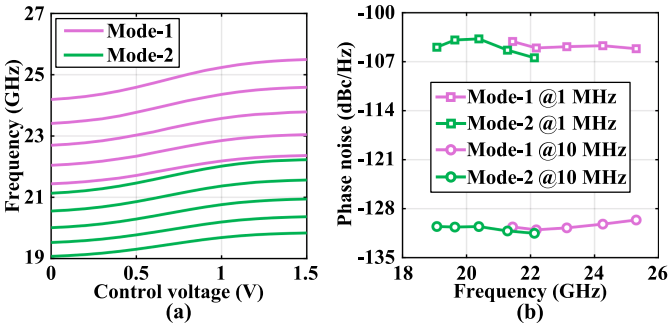

Fig. 8. Measured (a) frequency tuning and (b) phase noise of each mode.

TABLE I
COMPARISON WITH STATE-OF-THE-ART OSCILLATORS

Publication		**This work**	JSSC15 [15]	TMTT17 [5]	JSSC18 [24]	JSSC21 [25]	MWCL21 [10]
Architecture		**Dual-mode RTWO**	Quad-core LCO	Coupled LCO	Coupled RTWO	RTWO	Triple-mode LCO
Process		**40-nm CMOS**	40-nm CMOS	90-nm CMOS	28-nm CMOS	22-nm FD-SOI	180-nm CMOS
Frequency (GHz)		**19.1~25.5**	21.4~25.1	19.2~22.5	16.1~19.8	26.2~30.0	19.9~29.5
Tuning Range (%)		**28.7**	15.9	15.8	20.5	13.5	38.8
Power (mW)		**16.6~18.1**	23	8.1	75	21	14.4
Number of Phases		**16**	8	2	16	16	2
Core Area (mm^2)		**0.08**	0.06	0.09	0.38	0.24	0.04*
PN (dBc/Hz)	1 MHz	**−106.4 ~ −103.7**	−94.9	−100.7	−107.2*	−107.6	−97.6
	10 MHz	**−131.5 ~ −129.6**	−118.5	−124.3*	−132.5*	−128.9	−122.3
FoM (dBc/Hz)	1 MHz	**177.7~181.1**	168.6	177.8	173.5	184.1	175.4
	10 MHz	**185.1~186.2**	172.2	181.4	179.5	185.4	178.5
FoM$_T$ (dBc/Hz)	1 MHz	**186.8~190.3**	172.7	181.8	179.8	186.8	187.2
	10 MHz	**194.2~195.4**	176.3	185.4	185.7	188.1	190.3
FoM$_A$ (dBc/Hz)	1 MHz	**188.7~192.1**	180.8	188.2	177.7	190.3	189.4
	10 MHz	**196.1~197.2**	184.4	191.8	183.7	191.6	192.5

*Estimated from the figures in references FoM = $-PN(\Delta f) + 20\log_{10}(f_0/\Delta f) - 10\log_{10}(P_{DC}/1\text{mW})$
FoM$_T$ = FoM + $20\log_{10}$(TR / 10) FoM$_A$ = FoM − $10\log_{10}$(Area / 1mm^2)

are realized by the top thick metals. To reduce unnecessary coupling of the transmission lines between the left and right parts, a ground shield is placed in the middle of the structure. The simulated coupling coefficient k ($k = M/L_0$) is 0.45. Each RTWO core includes eight pairs of back-to-back inverters, providing the 16-phase output signals. The size of pMOS and nMOS used by inverters are is 32 μm/40 nm and 16 μm/40 nm, respectively. The simulated result shows that the dual-mode RTWO can start up within 1 ns in each mode. One pair of varactors and four differential switched capacitors are connected to each inverter to achieve frequency tuning in each mode. The mode switch is realized by nMOS with a size of 4 μm/40 nm. R_{ON} is about 75 Ω, which can effectively select the desired resonant mode.

IV. EXPERIMENTAL RESULT

Fig. 6 shows the die micrograph of the dual-mode RTWO. The core area is 200 μm × 400 μm. The frequency and phase noise of the dual-mode RTWO are measured by Rohde & Schwarz FSWP50. The proposed oscillator operates in mode-1 (21.5–25.5 GHz) and mode-2 (19.1–22.2 GHz) without observable stability problem. Then a continuous TR of 28.7% is obtained. Fig. 7 shows the measured phase noise at two typical frequencies of the two modes. The measured 1- and 10-MHz phase noise at 25.30 GHz is −105.14 and −129.62 dBc/Hz, respectively. For mode-2 operated at 22.12 GHz, the measured phase noise at 1- and 10-MHz offset is −106.44 and −131.52 dBc/Hz, respectively. The measured frequency tuning and phase noise of each mode are shown in Fig. 8. The power consumption is 16.6–18.1 mW from a 1.1-V supply. The measured supply pushing in mode-1 and mode-2 is 500 and 840 MHz/V, respectively. The measured results are summarized and compared with the state-of-the-arts in Table I. Chen and Chin [10] perform the widest frequency range using triple modes. However, it cannot support multiple phases, and the phase noise is much worse than our work. The proposed oscillator has obvious advantages in multiphase generation and highest overall performance of FoM$_T$ and FoM$_A$.

V. CONCLUSION

This letter proposes a dual-mode RTWO based on mode switching technique. The oscillator consists of two mutually nested and coupled RTWO cores. The coupling direction is controlled by mode switches to achieve dual-mode switching without worsening the quality factor. Verified in a 40-nm CMOS technology, the proposed dual-mode RTWO exhibits a 28.7% frequency from 19.1 to 25.5 GHz. With the wide TR, low phase noise, and small area, such RTWO is attractive for wideband and high-purity multiphase clock generation.

REFERENCES

[1] S.-L. Liu, K.-H. Chen, and A. Chin, "A dual-resonant mode 10/22-GHz VCO with a novel inductive switching approach," *IEEE Trans. Microw. Theory Techn.*, vol. 60, no. 7, pp. 2165–2177, Jul. 2012.

[2] J. Zhang, N. Sharma, and K. K. O, "21.5-to-33.4 GHz voltage-controlled oscillator using NMOS switched inductors in CMOS," *IEEE Microw. Wireless Compon. Lett.*, vol. 24, no. 7, pp. 478–480, Jul. 2014.

[3] Y.-H. Chang, Y.-C. Chiang, and C.-Y. Yang, "A V-band push-push VCO with wide tuning range in 0.18 μm CMOS process," *IEEE Microw. Wireless Compon. Lett.*, vol. 25, no. 2, pp. 115–117, Feb. 2015.

[4] Z.-Y. Yang and R. Y. Chen, "High-performance low-cost dual 15 GHz/30 GHz CMOS LC voltage-controlled oscillator," *IEEE Microw. Wireless Compon. Lett.*, vol. 26, no. 9, pp. 714–716, Sep. 2016.

[5] Z. Chen *et al.*, "Linear CMOS LC-VCO based on triple-coupled inductors and its application to 40-GHz phase-locked loop," *IEEE Trans. Microw. Theory Techn.*, vol. 65, no. 8, pp. 2977–2989, Aug. 2017.

[6] Y. Shu, H. J. Qian, and X. Luo, "A 20.7–31.8GHz dual-mode voltage waveform-shaping oscillator with 195.8dBc/Hz FoM_T in 28nm CMOS," in *Proc. IEEE Radio Freq. Integr. Circuits Symp. (RFIC)*, Jun. 2018, pp. 216–219.

[7] Y. Peng, J. Yin, P.-I. Mak, and R. P. Martins, "Low-phase-noise wideband mode-switching quad-core-coupled mm-wave VCO using a single-center-tapped switched inductor," *IEEE J. Solid-State Circuits*, vol. 53, no. 11, pp. 3232–3242, Nov. 2018.

[8] M. H. Kashani, R. Molavi, and S. Mirabbasi, "A 2.3-mW 26.3-GHz G_m-boosted differential Colpitts VCO with 20% tuning range in 65-nm CMOS," *IEEE Trans. Microw. Theory Techn.*, vol. 67, no. 4, pp. 1556–1565, Apr. 2019.

[9] Y. Shu, H. J. Qian, and X. Luo, "A 2-D mode-switching quad-core oscillator using E-M mixed-coupling resonance boosting," *IEEE J. Solid-State Circuits*, vol. 56, no. 6, pp. 1711–1721, Jun. 2021.

[10] Y.-D. Chen and A. Chin, "A wide tuning-range triple-mode CMOS VCO using switched-tunable inductor," *IEEE Microw. Wireless Compon. Lett.*, vol. 31, no. 9, pp. 1063–1066, Sep. 2021.

[11] A. Mazzanti, M. Sosio, M. Repossi, and F. Svelto, "A 24GHz sub-harmonic receiver front-end with integrated multi-phase LO generation in 65nm CMOS," in *IEEE Int. Solid-State Circuits Conf. (ISSCC) Dig. Tech. Papers*, Feb. 2008, pp. 216–608.

[12] S. M. Bowers and A. Hajimiri, "Multi-port driven radiators," *IEEE Trans. Microw. Theory Techn.*, vol. 61, no. 12, pp. 4428–4441, Dec. 2013.

[13] H.-H. Hsieh, Y.-C. Hsu, and L.-H. Lu, "A 15/30-GHz dual-band multiphase voltage-controlled oscillator in 0.18-μm CMOS," *IEEE Trans. Microw. Theory Techn.*, vol. 55, no. 3, pp. 474–483, Mar. 2007.

[14] F. Zhao and F. F. Dai, "A capacitive-coupling technique with phase noise and phase error reduction for multi-phase clock generation," in *Proc. IEEE Custom Integr. Circuits Conf.*, Sep. 2014, pp. 1–4.

[15] M. Hekmat, F. Aryanfar, J. Wei, V. Gadde, and R. Navid, "A 25 GHz fast-lock digital LC PLL with multiphase output using a magnetically-coupled loop of oscillators," *IEEE J. Solid-State Circuits*, vol. 50, no. 2, pp. 490–502, Feb. 2015.

[16] X. Yi, C. C. Boon, G. Feng, and Z. Liang, "An eight-phase in-phase injection-coupled VCO in 65-nm CMOS technology," *IEEE Microw. Wireless Compon. Lett.*, vol. 27, no. 3, pp. 299–301, Mar. 2017.

[17] R. Jiang, H. Noori, and F. F. Dai, "A 2.33-GHz, -133-dBc/Hz, and eight-phase oscillator with dual tanks and adaptive feedback," *IEEE Trans. Microw. Theory Techn.*, vol. 66, no. 3, pp. 1399–1410, Mar. 2018.

[18] R. Jiang, H. Noori, and F. F. Dai, "A multi-phase coupled oscillator using inductive resonant coupling and modified dual-tank techniques," *IEEE J. Solid-State Circuits*, vol. 53, no. 9, pp. 2454–2464, Sep. 2018.

[19] L. Wu and Q. Xue, "E-band multi-phase LC oscillators with rotated-phase-tuning using implicit phase shifters," *IEEE J. Solid-State Circuits*, vol. 53, no. 9, pp. 2560–2571, Sep. 2018.

[20] J. Wood, T. C. Edwards, and S. Lipa, "Rotary traveling-wave oscillator arrays: A new clock technology," *IEEE J. Solid-State Circuits*, vol. 36, no. 11, pp. 1654–1665, Nov. 2001.

[21] J.-C. Chien and L.-H. Lu, "A 32-GHz rotary traveling-wave voltage controlled oscillator in 0.18-μm CMOS," *IEEE Microw. Wireless Compon. Lett.*, vol. 17, no. 10, pp. 724–726, Oct. 2007.

[22] N. Nouri and J. F. Buckwalter, "A 45-GHz rotary-wave voltage-controlled oscillator," *IEEE Trans. Microw. Theory Techn.*, vol. 59, no. 2, pp. 383–392, Feb. 2011.

[23] A. Moroni, R. Genesi, and D. Manstretta, "Analysis and design of a 54 GHz distributed 'hybrid' wave oscillator array with quadrature outputs," *IEEE J. Solid-State Circuits*, vol. 49, no. 5, pp. 1158–1172, May 2014.

[24] M. Vigilante and P. Reynaert, "A coupled-RTWO-based subharmonic receiver front end for 5G E-band backhaul links in 28-nm bulk CMOS," *IEEE J. Solid-State Circuits*, vol. 53, no. 10, pp. 2927–2938, Oct. 2018.

[25] M. A. Shehata, M. Keaveney, and R. B. Staszewski, "A distributed stubs technique to mitigate flicker noise upconversion in a mm-wave rotary traveling-wave oscillator," *IEEE J. Solid-State Circuits*, vol. 56, no. 6, pp. 1745–1760, Jun. 2021.